Available online at www.sciencedirect.com
ScienceDirect
Journal of Hazardous Materials 147 (2007) 997–1005
Journal of Hazardous Materials
www.elsevier.com/locate/jhazmat

Application of MCM-41 for dyes removal from wastewater

Chung-Kung Lee [a,*], Shin-Shou Liu [a], Lain-Chuen Juang [a], Cheng-Cai Wang [a], Kuen-Song Lin [b], Meng-Du Lyu [a]

[a] *Green Environment R&D Center and Department of Environmental Engineering, Vanung University, Chung-Li 320, Taiwan, ROC*
[b] *Department of Chemical Engineering and Materials Science/Fuel Cell Center, Yuan-Ze University, Chung-Li 320, Taiwan, ROC*

Received 17 July 2006; received in revised form 27 January 2007; accepted 29 January 2007
Available online 3 February 2007

Abstract

The adsorption of three basic dyes (Rhodamine B (RB), Crystal Violet (CV), and Methylene Green (MG)) and two acid dyes (Acid Red 1 (AR1) and Erioglaucine (EG)) onto MCM-41 was studied to examine the potential of MCM-41 for the removal of dyes from water solution. The revolution of pore structure and surface chemical characteristics of MCM-41 induced by dyes adsorption was characterized based on the analyses of XRD patterns, FTIR spectra, and nitrogen adsorption–desorption isotherms. The adsorption capacity of MCM-41 for the five dyes followed a decreasing order of RB > CV > MG > EG ~ AR1. It was experimentally concluded that if the dyes adsorption did not introduce a serious disorder on the pore structure of MCM-41 (such as RB adsorption), MCM-41 might be a good adsorbent for the removal of basic dyes from water solution. The fitness of both Langmuir and Freundlich adsorption model on describing the equilibrium isotherms of three basic dyes was examined. The suitability of both pseudo-second-order kinetic model and the intraparticle diffusion model for the description of the kinetic data was investigated, from which the adsorption mechanism was examined.

Keywords: MCM-41; Dyes; Adsorption; Pore structure stability

1. Introduction

Dye wastewaters are discharged by a wide variety of sources, such as textiles, printing, dyeing, dyestuff manufacturing, and food plants [1–3]. They are the important sources of water pollution due to some dyes and their degradation products may be carcinogens and toxic to mammals [4,5]. Moreover, the color produced by organic dyes in water is of great concern because the color in water is aesthetically unpleasant. Some investigations have been conducted on the physical, chemical, and biological methods of removing color from dye wastewater [6–8]. For the examined methods, it was found that physical adsorption might be an efficient and economic process to remove dyes and also to control the bio-chemical oxygen demand [9]. Numerous studies have been devoted to the dyes adsorption mechanism and to the search for a suitable adsorbent [10]. The application of adsorption technology utilizing commercial activated carbon has become known and taken a place as one of the most effective technologies for the removal effluents of dyes [11,12]. However, activated carbon often suffers from high-cost production and regeneration. Therefore, other materials such as some natural adsorbents (e.g., clays and clay minerals, cellulosic materials, chitin, and chitosan), certain waste materials, and some agricultural by-products are alternatives [13–18]. In recent years, mesoporous molecular sieves, such as surfactant-modified FSM-16 [19], MCM-22 [20], and silane-modified MCM-41 [21], have been accepted as one of the appropriate adsorbents for the removal of dyes from wastewater due to their unique mesoporous pore structure characterized by high surface area and pore volume.

MCM-41 is a novel mesoporous zeolite, synthesized by Mobil researchers in 1992 [22]. It is characterized by parallel and ideally shaped pore structures without the complications of a network. The cylindrical pore structure and high degree of pore symmetry found in MCM-41 have made it an ideal candidate for testing various existing adsorption and diffusion models [23]. Moreover, its large surface area and nanometer-sized pore sizes (from 20 to 100 Å) [22] also offer a special environment for chemical separations of large molecules (such as dyes). In the present study, our objective is to examine the potential of

* Corresponding author. Tel.: +886 34515811x718; fax: +886 34622232.
E-mail address: anthony@msa.vnu.edu.tw (C.-K. Lee).

0304-3894/$ – see front matter © 2007 Elsevier B.V. All rights reserved.
doi:10.1016/j.jhazmat.2007.01.130

MCM-41 for the removal of dyes from water solution by measuring the adsorption data of basic and acid dyes. It is well known that silicate materials, such as MCM-41, have a negative charge density due to the presence of Si–O and Si–OH groups, which should adsorb positive charged dyes and do not permit the adsorption of the negative ones [24]. However, it is found from the literature [21] that the adsorption capacity of both acid and basic dyes on pure MCM-41 is very low, indicating that other factors (such as structure stability of MCM-41 during the adsorption process) must be considered for dyes adsorption on MCM-41 in addition to the factor of negative charge density. Accordingly, three basic dyes (RB, CV, and MG) with different molecular configurations are selected as testing adsorbates to examine the effects of basic dyes adsorption on the pore structure stability of MCM-41. Moreover, for giving a more comprehensive study, two acid dyes (AR1 and EG) are also included. The changes of pore structure and surface chemical characteristics of MCM-41 introduced by dyes adsorption are characterized based on the analyses of XRD patterns, FTIR spectra, and nitrogen adsorption–desorption isotherms. The equilibrium data are fitted into Langmuir and Freundlich equations to determine the correlation between the isotherm models and experimental data. The thermodynamic and kinetic parameters are calculated to determine the adsorption mechanism.

2. Materials and adsorption isotherms

2.1. Adsorbent

The mesoporous MCM-41 powder was crystallized from an alkaline solution containing cetyltrimethylammonium bromide (CTABr, 99%, Merck), sodium silicate solution (Na_2O, 7.5–8.5%, SiO_2, 25.8–28.5%, Merck), sulfuric acid (98%, Merck), and deionized water in the mole ratio of $1CTABr:1.76Na_2O:6.14SiO_2:335.23H_2O:1.07H_2SO_4$. After 24 h of crystallization at room temperature, the MCM-41 powder was filtered, washed, and dried before it was calcined in a furnace at 450 °C for 4 h to remove the organic template.

2.2. Adsorbates

Three basic dyes (RB, CV, and MG) and two acid dyes (AR1 and EG) were selected as adsorbates to discuss the adsorption selectivity of MCM-41 in terms of pore structure and surface charge density of adsorbent and molecular shape of adsorbates. All compounds were of analytical grade from Sigma Chemical Co. (USA) and were used without further purification. Their chemical structures were shown in Fig. 1.

2.3. Adsorption measurements

The dye adsorption data from water solutions were obtained by the immersion method. All dye adsorbates were first dried at 105 °C for 24 h to remove moisture before use. All of the dye solution was prepared with distilled water. For adsorption experiments, 0.1-g-MCM-41 was added into 100 ml of dye water solutions at the desired concentration. The initial pH value of the solution was adjusted with NaOH or HCl solution to reach a desirable value. The preliminary experiment revealed that about 3 h was required for the adsorption process to reach equilibrium with a reciprocating shaker equipped with a constant temperature controller and a cover to keep isothermal condition. The solution and solid phase were separated by centrifugation at 8000 rpm for 25 min in a Sorvall RC-5C centrifuge. A 15-ml aliquot of the supernatant was removed and analyzed for RB, CV, MG, AR1 and EG by UV (Hitachi, U-2000) at the wave length of 555, 589, 655, 530, and 630 nm, respectively. The adsorption capacity of dyes was then calculated using the relation $Q = V\Delta C/m$, where V was the volume of the liquid phase, m was the mass of MCM-41, and ΔC was the difference between the initial and final concentration of dye in solutions, which could be computed simply from the initial and final UV readings. For the adsorption kinetics experiments, the dye adsorption amounts were determined by analyzing the solution at appropriate time intervals.

The effects of temperature and pH on the adsorption data were carried out by performing the adsorption experiments at various temperatures (25, 45, and 65 °C) and various initial pHs (2–11), respectively.

A zeta potential analyzer (Zetasizer, 3000HS, Malvern Co.) was used to measure the zeta potential of MCM-41 at different pH values. At least three runs were conducted for each sample and the average value was recorded. The phase structure of the MCM-41 samples before and after adsorbing dyes were evaluated from the XRD patterns obtained from Thermal ARL X-ray diffractometer equipped with a Cu Kα radiation source and a graphite monochromator. FTIR spectra of MCM-41 samples were recorded using a Perkin-Elemer Model 1600 FTIR spectrophotometer over the range 4000–400 cm^{-1}. IR spectra were obtained in KBr disks. The porous structure characteristics of MCM-41 samples, including surface area and pore volume, were obtained from the conventional analysis of nitrogen adsorption–desorption isotherms measured at 77 K with Micromeritics TriStar 3000 apparatus.

3. Results and discussion

3.1. Adsorption of different dyes

Fig. 2 shows pH effects on the adsorption capacity of five different dyes on MCM-41. For MG and CV, the adsorption capacity are measured under $pH < 8$ because both dyes may decompose when $pH > 8$. One can see that the adsorption capacity of RB decreases significantly at low (2–4) and high (9–11) pHs. The MG also shows an obvious decrease in the adsorption capacity at low pHs (2–4). Moreover, at pHs 3–7 the adsorption capacity of five dyes follows a decreasing order of $RB > CV > MG > EG \sim AR1$.

As shown in Fig. 3 for the dependence of zeta potential of MCM-41 on pHs, the surface charge of MCM-41 is negative at all examined pHs. Moreover, although the zeta potential changes obviously at pHs 4–8, the variation of zeta potential of MCM-41 at different pHs is slight from an overall view point and the effects of pHs on the adsorption capacity of basic dyes may be

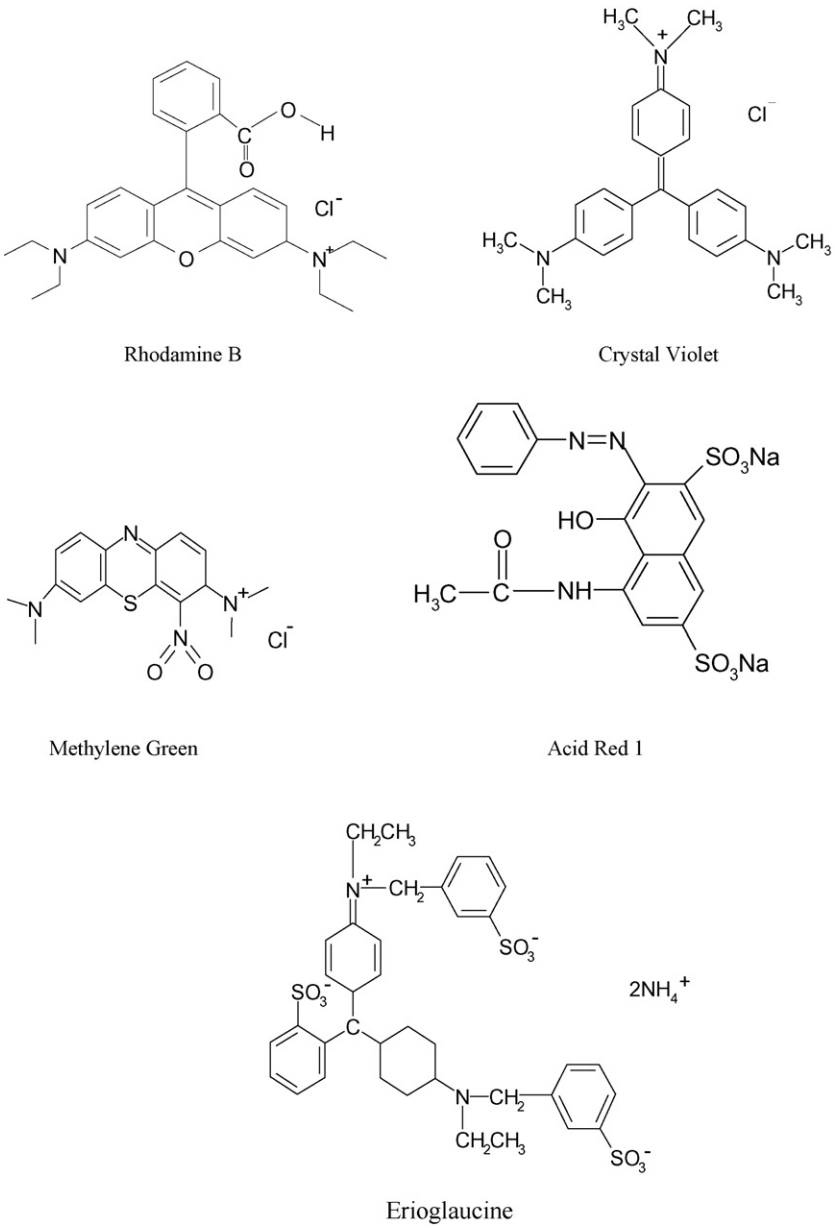

Fig. 1. Chemical structures of examined dyes.

small. The obvious decrease in the adsorption capacity of RB and MG at high or low pHs may be due to the decrease in the structure stability of MCM-41 (such as the dissolution of MCM-41) [21]. On the other hand, the low and high adsorption capacity of acid (EG and AR1) and basic dyes (RB, CV, and MG) on MCM-41 can be explained with the existence of repulsive and attractive forces between the dyes and MCM-41, respectively. However, the significant difference existing in the adsorption capacity of three basic dyes is difficult to explain only from the variation of molecular size. One way to interpret the above result may be with the aid of the revolution of structure stability of MCM-41 during the basic dyes adsorption process, which is also closely related to the difference existing in the interactions between dyes and surface hydroxyl groups of MCM-41 [25]. In general, it is found that the interactions between the incorporated dye molecules and MCM-41 are very strong [26–28]. This may induce a serious disorder in the pore structure of MCM-41, and then create a sharp decrease in the adsorption capacity. In the following paragraphs, the revolutions of pore structure and surface chemical characteristics of MCM-41 before and after adsorbing dyes are examined with the analysis of XRD patterns, FTIR spectra, and nitrogen adsorption–desorption isotherms to give some supports on the above deduction.

The XRD patterns of MCM-41 accompanied with the adsorption processes are demonstrated in Fig. 4. The presence of both (1 0 0) and (2 0 0) diffraction peaks in the primary MCM-41 is an evidence of good crystallinity of the prepared powder. However, a severe modification of the phase structure emerges from Fig. 4 after adsorbing dyes. If the diffraction patterns are compared, it is clearly observed that the adsorption of CV, MG, AR1, and EG

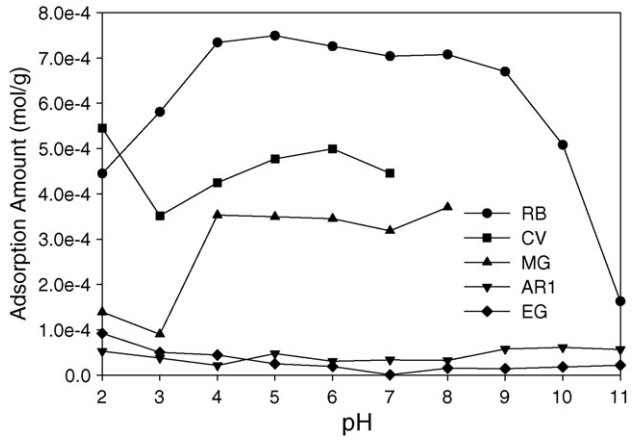

Fig. 2. Effect of pH on dyes adsorption onto MCM-41 at 25 °C and dye initial concentration 900 mg/l.

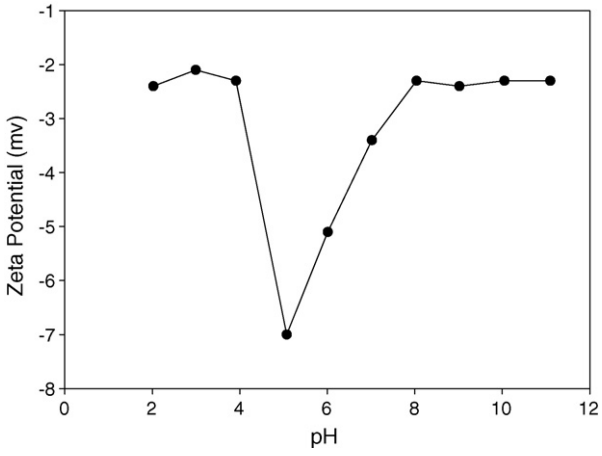

Fig. 3. Dependence of zeta potential of MCM-41 on pH values.

has induced a serious disorder in the pore structure of MCM-41, as indicated by the sharp decrease in the intensity of most MCM-41 peaks. Infrared spectra of MCM-41 before and after adsorbing dyes are demonstrated in Fig. 5. As shown in Fig. 5,

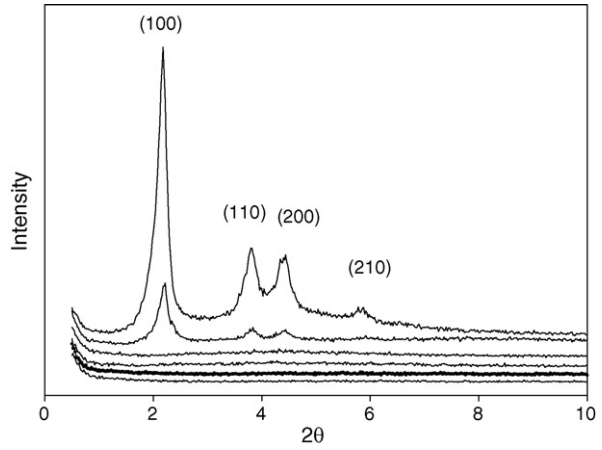

Fig. 4. XRD patterns of the MCM-41s before and after adsorbing dyes; from bottom to top is AR1/MCM-41, EG/MCM-41, MG/MCM-41, CV/MCM-41, RB/MCM-41, and MCM-41. Conditions: pH 4, 25 °C, and dye initial concentration 900 mg/l.

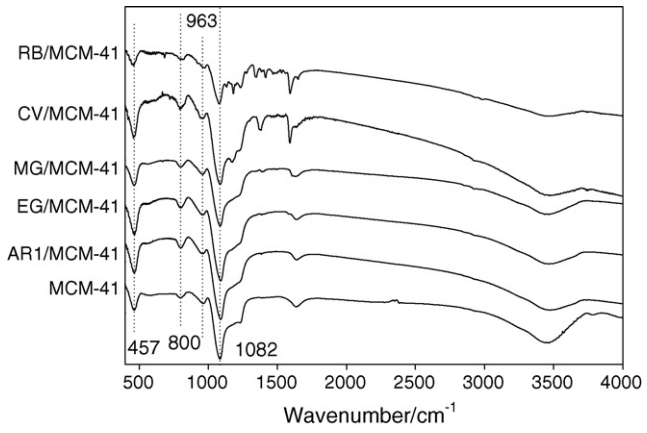

Fig. 5. FTIR spectra of the MCM-41 before and after adsorbing dyes; from bottom to top is MCM-41, AR1/MCM-41, EG/MCM-41, MG/MCM-41, CV/MCM-41, and RB/MCM-41. Conditions: pH 4, 25 °C, and dye initial concentration 900 mg/l.

the three well-known vibrational modes of a-SiO_2 are visible in all spectra [28]. These are the rocking mode near 457 cm^{-1}, the symmetrical stretching mode near 800 cm^{-1}, and the asymmetric stretching mode near 1082 cm^{-1} in which the oxygen atom vibrates along a line parallel to a line joining the adjacent silicon atoms. Moreover, the characteristic absorption peak of MCM-41 around 963 cm^{-1} is also observed for all MCM-41 samples, indicating the change in the pore structure of MCM-41 induced by the dyes adsorption is more likely due to the inherent disorder but not the collapse of the MCM-41 mesoporous structure.

For providing more information about the structure changes of MCM-41 during basic dyes adsorption process, the nitrogen adsorption–desorption isotherms are also measured, as shown in Fig. 6. Some key features may be found directly from this figure. It can be seen that the monolayer capacity, thus the BET surface area of MCM-41, becomes smaller when basic dyes are adsorbed. This result implies that the large basic dyes may screen some MCM-41 surface rugosity and clog some smaller pores, which becomes inaccessible for the nitrogen molecule

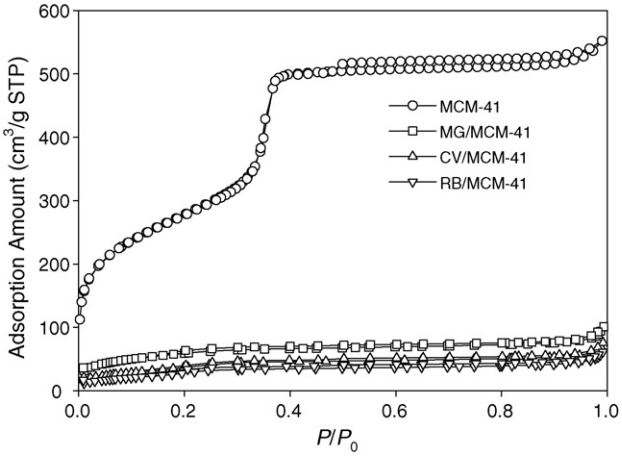

Fig. 6. Nitrogen adsorption isotherms of MCM-41s before and after adsorbing basic dyes. Conditions: pH 4, 25 °C, and dye initial concentration 900 mg/l.

Table 1
Specific surface areas, specific pore volumes, and average pore diameters of MCM-41s before and after adsorbing basic dyes

Solid	BET surface area (m^2/g)	Average pore diameter (nm)	Total pore volume (cm^3/g)
MCM-41	1003.5	3.96	0.76
RB/MCM-41	99.2	1.41	0.05
MG/MCM-41	213.6	–	0.07
CV/MCM-41	131.8	–	0.07

and inhibits the passage of nitrogen molecules into these pores, respectively. Another key feature in Fig. 6 is that primary MCM-41 shows clear capillary condensation at moderate nitrogen pressure. However, the capillary condensation phenomenon becomes diffuse when basic dyes are adsorbed on MCM-41, signifying the adsorption process may decrease the pore sizes uniformity. The pore sizes can be calculated from the X-ray diffraction interplanar spacing (Fig. 4) and nitrogen isotherms (Fig. 6) using the equation,

$$S = bd\left(\frac{\rho V_p}{(1+\rho V_p)}\right)^{1/2} \quad (1)$$

where S is the pore size, b is a constant dependent on the assumed pore geometry and is equal to 1.155 for hexagonal models, d is the XRD(1 0 0) interplanar spacing, V_p is the mesoporous volume, and ρ is the pore wall density (ca. 2.2 cm^3/g for siliceous materials) [29]. It is noteworthy that the average pore sizes of both MG/MCM-41 and CV/MCM-41 are difficult to estimate because the (1 0 0) peak does not exist in Fig. 4. As listed in Table 1, the adsorption of RB may decrease the pore size of MCM-41 to some extent. Finally, the saturation adsorption capacity shown in Fig. 6 also suggests an enormous decrease in the total pore volume of MCM-41 after basic dyes are adsorbed (see also Table 1). Obviously, the adsorption process of basic dyes leads to the simultaneous decrease in the specific surface area, pore size, and pore volume of MCM-41.

According to the adsorption capacity and the analysis of XRD patterns, FTIR spectra, and nitrogen adsorption–desorption isotherms, it is experimentally demonstrated that the adsorption capacity of basic dyes is closely related to the pore structure stability of MCM-41 during the adsorption process. If the inherent disorder (in the pore structure of MCM-41) induced by basic dyes adsorption is insignificant (e.g., RB adsorption), MCM-41 may be a good adsorbent for the removal of basic dyes even if no chemical modification on MCM-41 is taken.

In the following section, the discussion in the adsorption isotherms and kinetics for providing more information about the adsorption mechanism of dyes adsorption onto MCM-41 is given. The work described here will focus on the three basic dyes as the adsorption capacity of acid dyes is very low.

3.2. Adsorption isotherms of basic dyes

It is well known that activated carbon is often selected as an adsorbent for the adsorptive removal of dyes from wastewater solutions. On the other hand, montmorillonite is also an ideal adsorbent for removal of basic dyes since it possesses the capability of interlamellar expansion and high cation exchange capacity [7], from which high amounts of basic dyes can be adsorbed with the cation exchange process. For MCM-41, it also possesses negative surface charge density but with the incapability of expansion of its cylindrical pore. Therefore, it is an interesting task to compare the adsorption capacity of basic dyes on the activated carbon, montmorillonite, and MCM-41, from which the potential of MCM-41 as an adsorbent for the removal of basic dyes can also be examined. The adsorption isotherms of RB on the activated carbon (purchased from Merck), Ca-montmorillonite (SAz-1, purchased from the University of Missouri-Columbia, Source Clay Minerals Repository), and MCM-41 at 25 °C are demonstrated in Fig. 7. As shown in Fig. 7, MCM-41 possesses the largest capacity among the three adsorbents, indicating MCM-41 may be an attractive adsorbent for the removal of basic dyes from wastewater.

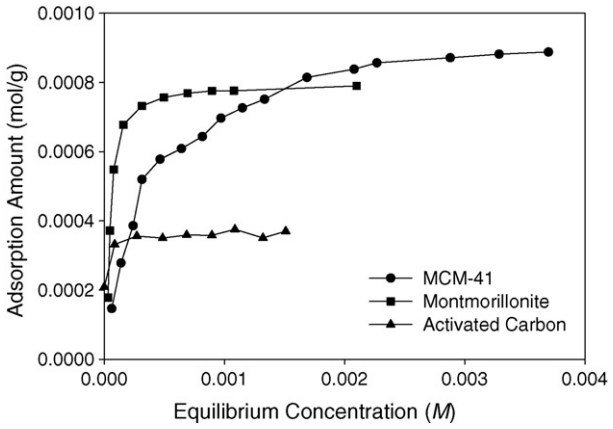

Fig. 7. Comparison of adsorption isotherms of RB on activated carbon, Ca-montmorillonite, and MCM-41 at 25 °C.

Fig. 8 shows RB, CV, and MG adsorption isotherms at different temperatures. As can be seen the adsorption capacity of basic dyes on MCM-41 is largely perceptible to temperature changes and the isotherm types can be divided into two cases: type I (RB) and type IV (CV and MG). As mentioned earlier, the adsorption of both CV and MG may introduce a serious disorder in the pore structure of MCM-41. Accordingly, the change in the adsorption isotherm type may be closely related to the effect of basic dyes adsorption on the pore structure stability of MCM-41.

The equilibrium adsorption isotherm is of importance in the design of adsorption systems. For MCM-41, its cylindrical pore structure is assumed to be high degree of pore symmetry and the adsorption environment in MCM-41 may be viewed as a homogeneous system. However, if the adsorption causes a serious disorder in the pore structure of MCM-41, the adsorption environment may become a heterogeneous system. Accordingly, the equilibrium adsorption data are fitted into the model of Langmuir and Freundlich. The Langmuir equation is applicable to homogeneous adsorption system [30], while the Freundlich equation is an empirical equation employed to describe heterogeneous systems and is not restricted to the formation of the monolayer [31].

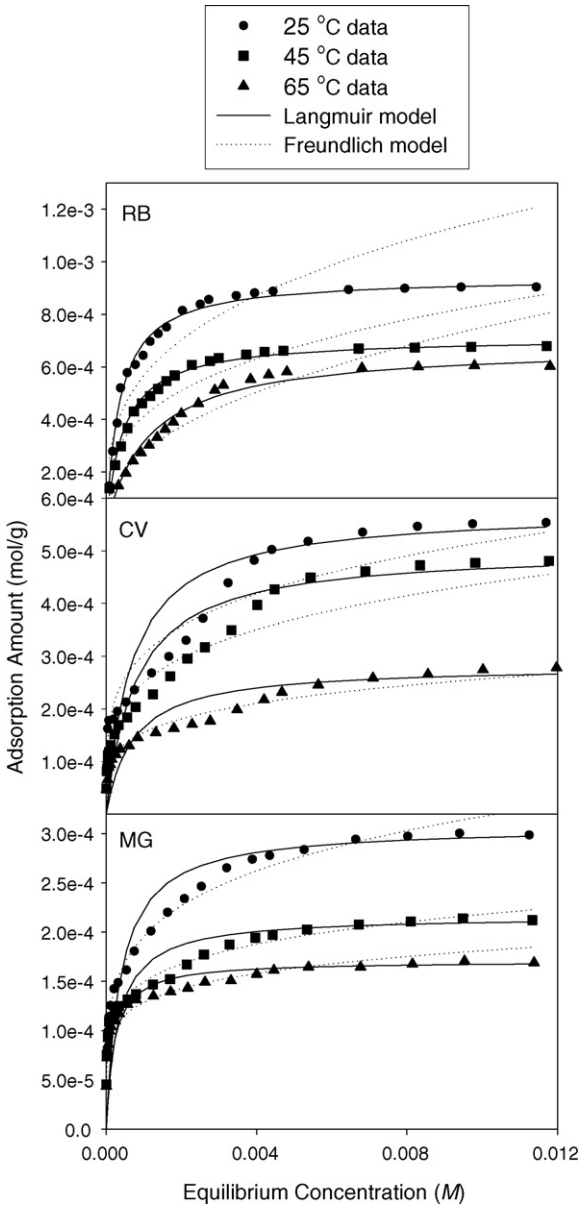

Fig. 8. Langmuir and Freundlich adsorption isotherms of RB, CV, and MG on MCM-41 at different temperatures and pH 4.

The well known Langmuir equation is represented as

$$\frac{C_e}{Q_e} = \frac{1}{Q_{max} K_L} + \frac{C_e}{Q_{max}}, \quad (2)$$

where Q_e is the equilibrium basic dyes concentration on the adsorbent (mol/g), C_e is the equilibrium basic dyes concentration in solution (mol/l), Q_{max} is the monolayer capacity of MCM-41 (mol/g), and K_L is the Langmuir adsorption constant (l/mol) related to the free energy of adsorption. The Langmuir constant K_L is a measure of the affinity between adsorbate and adsorbent and its reciprocal value gives the concentration at which half the maximum adsorption capacity of the adsorbent is reached [30]. A plot of C_e/Q_e versus C_e will give a straight line with slope $1/Q_{max}$ and intercept $1/Q_{max}K_L$, if Langmuir model is held. On the other hand, the Freundlich equation is represented as

$$Q_e = K_F C_e^{1/n}, \quad (3)$$

where K_F ((mol/g(l/mol)$^{1/n}$)) and $1/n$ are the Freundlich constants corresponding to adsorption capacity and adsorption intensity, respectively [31]. The plot of $\ln Q_e$ versus $\ln C_e$ is employed to generate the intercept K_F and the slope $1/n$. The fitting results of both Langmuir and Freundlich models are shown in Fig. 8 and the values of K_L, Q_{max}, K_F, $1/n$, and the linear regression correlations are given in Table 2. As listed in Table 2, Langmuir model should better describe the three basic dyes adsorption on MCM-41 than Freundlich model. Moreover, the adsorption of three basic dyes on MCM-41 is largely perceptible to temperature changes, as shown in the variation of both Q_{max} and K_L with temperatures. On the other hand, the values of $1/n$ are all less than 1 at all temperatures, indicative of high adsorption intensity. If the K_F values are compared at all temperatures studied, it is found that lower values of K_F are obtained at higher temperatures, indicating that basic dyes possess higher adsorption capacity at lower temperatures.

Although Langmuir model gives a better fitting result than Freundlich model, it should be noted that the dependence of K_L on the temperature for both MG and CV violates the thermodynamic consistency. For MG and CV, the increase in the K_L values with increasing temperatures indicates that the adsorption process is endothermic process. However, Fig. 8 shows that adsorption capacities for all tested dyes augment with a decrease of temperature. This fact indicates that adsorption process is an exothermic process and implies that the Langmuir model is not appropriate for the description of both MG and CV adsorption onto MCM-41 although its fitting result is good from a mathematical point of view. The fail of Langmuir model for describing the adsorption of MG and CV may be ascribed to the serious disorder in the pore structure of MCM-41 induced by the two basic dyes adsorption, from which the adsorption environment may become heterogeneous and the adsorption isotherms are not type I but with type IV. In such case, Freundlich model may be more appropriate for description of adsorption isotherms than Langmuir model.

Adsorption is accompanied by evolution of heat since adsorbates are more stabilized on the adsorbent surface than in the bulk phase. Since adsorption is an exothermic process, the concentration of the adsorbed material decreases with increased temperature at a given equilibrium concentration, as the basic dyes isotherms of Fig. 8 indicate. The temperature dependency of Henry's constant K obeys the van't Hoff equation [32]:

$$\frac{d \ln K}{dT} = \frac{\Delta H}{RT^2} \quad (4)$$

where R is the gas constant and T is the temperature (in Kelvin). Eq. (4) can be integrated to yield $\ln K = \ln K_0 + (-\Delta H/RT)$. A plot of $\ln K$ versus $1/T$ will yield a straight line with a slope of $-\Delta H/R$. The heats of adsorption, calculated from the slope, are -32.1 ± 4.2, -7.5 ± 2.9, and -26.3 ± 0.3 kJ/mol for RB, MG, and CV, respectively.

Table 2
Langmuir and Freundlich isotherm constants for the adsorption of RB, MG, and CV onto MCM-41

T (°C)	Dye	Langmuir			Freundlich		
		Q_{max} (mol/g)	K_L (l/mol)	r_L^2	$1/n$	K_F (mol/g(l/mol)$^{1/n}$)	r_F^2
25	RB	9.4×10^{-4}	3.3×10^{3}	0.999	0.310	5.100×10^{-3}	0.823
45		7.1×10^{-4}	2.7×10^{3}	0.999	0.306	3.623×10^{-3}	0.877
65		6.8×10^{-4}	1.0×10^{3}	0.995	0.434	5.983×10^{-3}	0.935
25	MG	3.1×10^{-4}	2.7×10^{3}	0.997	0.208	8.292×10^{-4}	0.992
45		2.2×10^{-4}	3.2×10^{3}	0.996	0.163	4.620×10^{-4}	0.988
65		1.7×10^{-4}	5.0×10^{3}	0.998	0.148	3.576×10^{-4}	0.958
25	CV	5.8×10^{-4}	1.5×10^{3}	0.980	0.229	1.479×10^{-3}	0.957
45		5.0×10^{-4}	1.3×10^{3}	0.980	0.242	1.333×10^{-3}	0.947
65		2.8×10^{-4}	1.4×10^{3}	0.980	0.216	6.951×10^{-4}	0.978

3.3. Adsorption kinetics of basic dyes

The effect of contact time on the amount of RB, CV, and MG adsorbed onto MCM-41 was measured at the optimum initial concentration and different temperatures. A simple kinetic analysis was performed with the aid of pseudo-second-order equation [33]. In this equation, the value of the rate constant k can be calculated in the form

$$\frac{dQ_t}{dt} = k(Q_e - Q_t)^2 \quad (5)$$

where Q_e and Q_t are the amount of dye adsorbed per unit mass of the adsorbent at equilibrium and time t, respectively. After definite integration by applying the initial conditions $Q_t = 0$ at $t = 0$ and $Q_t = Q_t$ at $t = t$, Eq. (5) becomes

$$\frac{t}{Q_t} = \frac{1}{kQ_e^2} + \frac{1}{Q_e}t. \quad (6)$$

The plot of t/Q_t versus t gives straight lines. Linear plots of the t/Q_t versus t with linear regression coefficients higher than 0.99 indicates the applicability of this kinetic equation and the pseudo-second nature of the adsorption process of three basic dyes onto MCM-41. Fig. 9 presents the plots for the adsorption of three basic dyes on MCM-41 using the pseudo-second-order kinetic model. Table 3 lists the kinetic parameters obtained from the pseudo-second-order model and it is seen that the equilib-

Table 3
Parameters of kinetic model of RB, CV, and MG adsorption onto MCM-41. Conditions: initial dye concentration 900 mg/l and pH 4

T (°C)	Dye	Pseudo-seconder-order model		
		k (g/mol min)	Q_e (mol/g)	R^2
25	RB	320.9	8.2×10^{-4}	0.999
45		1239.3	6.6×10^{-4}	0.999
65		7951.6	5.5×10^{-4}	0.999
25	CV	302.4	3.3×10^{-4}	0.999
45		564.2	2.6×10^{-4}	0.999
65		327.1	1.8×10^{-4}	0.999
25	MG	296.6	2.9×10^{-4}	0.999
45		505.3	1.7×10^{-4}	0.999
65		444.2	1.2×10^{-4}	0.999

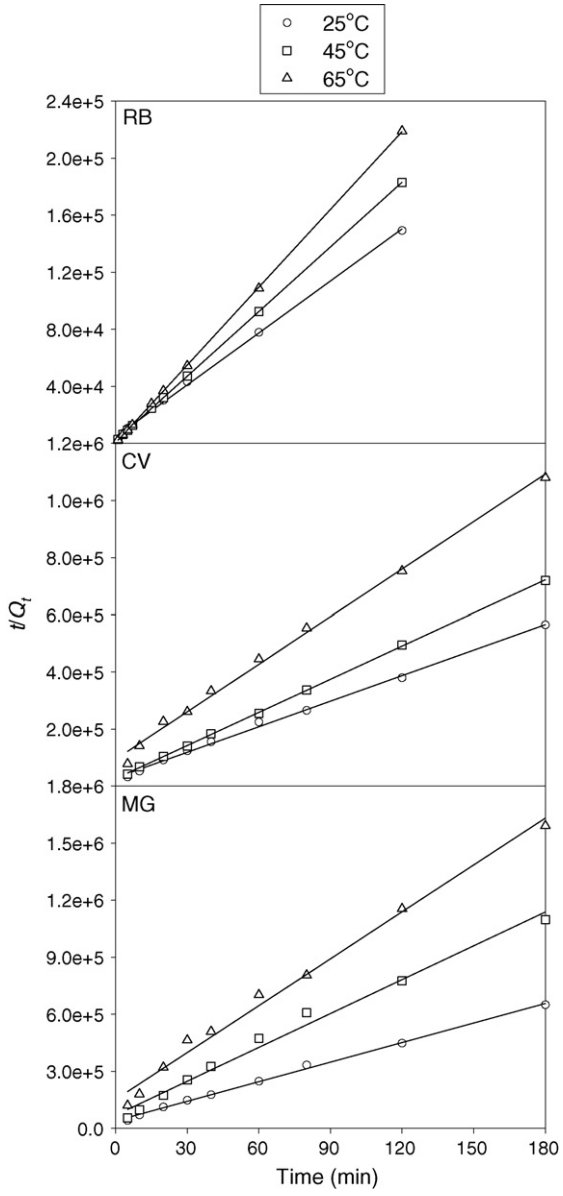

Fig. 9. Comparison of pseudo-second-order kinetics of RB, CV, and MG adsorption on MCM-41. Conditions: initial dyes concentration 900 mg/l, 25 °C, and pH 4.

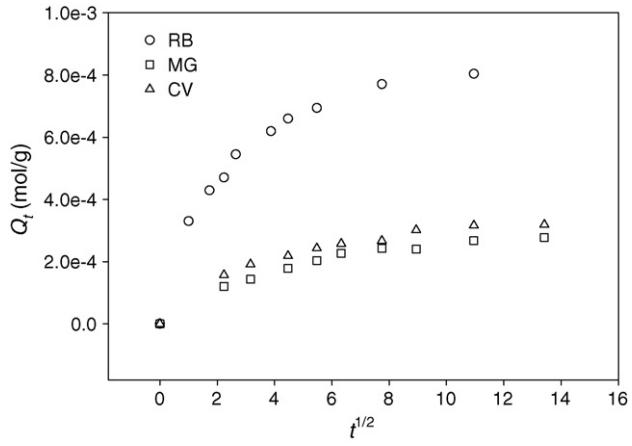

Fig. 10. The diffusion model plots for the adsorption of RB, CV, and MG on MCM-41. Conditions: initial dyes concentration 900 mg/l, 25 °C, and pH 4.

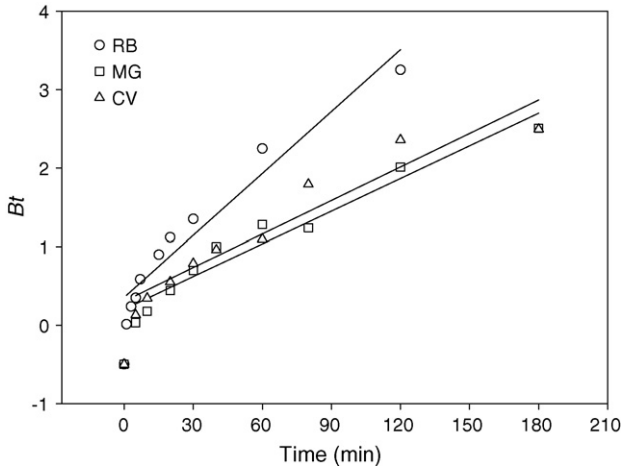

Fig. 11. Correlation between Bt and t for RB, CV, and MG adsorption onto MCM-41.

rium adsorption capacity (Q_e) shows a slight decrease with the increasing temperature. From the k values it is observed that for RB (CV and MG), temperature effect on the adsorption kinetics is (not) significant.

In addition to the pseudo-second-order rate equation, the intraparticle diffusion model is commonly used technique for identifying the steps involved during adsorption, described by external mass transfer (boundary-layer diffusion) and intraparticle diffusion [20]. The intraparticle diffusion model is expressed as

$$Q_t = k_d(t^{1/2}) \tag{7}$$

where k_d is the diffusion coefficient. Fig. 10 presents the typical plots for the adsorption of three basic dyes on MCM-41 using diffusion model. As shown in Fig. 10, the two-phase plot suggests that the adsorption process proceeds by surface adsorption and intraparticle diffusion, namely, the initial curved portion of the plot indicates a boundary-layer effect while the second linear portion is due to intraparticle or pore diffusion.

Because the double nature of intraparticle diffusion plot confirms the presence of film and pore diffusion, the adsorption kinetic data can be further analyzed using Boyd kinetic expression (Eq. (8)) to determine the actual rate-controlling step involved in the dye adsorption process [34].

$$F = 1 - \frac{6}{\pi^2}\exp(-Bt) \tag{8}$$

$$B = \frac{\pi D}{r^2} = \text{time constant} \tag{9}$$

where D is the effective diffusion coefficient of adsorbates in adsorbent phase, r is the radius of adsorbent particle assumed to be spherical, and F is the fraction of solute adsorbed at different times t and given by

$$F = \frac{Q_t}{Q_e} \tag{10}$$

where Q_t and Q_e represent the amount adsorbed (mol/g) at any time t and at infinite time. In this work, we take Q_e from the second-order kinetic model, as listed in Table 3. Substituting Eq. (10) into Eq. (8), the kinetic expression becomes

$$Bt = -0.4977 - \ln\left(1 - \frac{Q_t}{Q_e}\right). \tag{11}$$

Thus, the value of Bt can be calculated for each t value. Fig. 11 shows the calculated Bt values against time for RB, CV, and MG at 25 °C. The linearity of this plot will provide useful information for distinguishing between external-transport- and intraparticle-transport-controlled rates of adsorption [35]. In general, if a plot of Bt versus t is a straight line passing through the origin, then adsorption is governed by a particle-diffusion mechanism, otherwise it is governed by film diffusion. From Fig. 11, it is observed that the plots are not straight lines to pass the origin (the R^2 of linear fitting for RB, MG, and CV is 0.9452, 0.9493, and 0.9211, respectively), implying external mass transport mainly governs the rate-limiting process. Several previous investigations have reported a similar type of pattern for dyes adsorption on activated carbon [36], fly ash [37], rice husk [35], and MCM-22 [20].

4. Conclusions

It is experimentally concluded that if the pore structure stability of MCM-41 could be maintained during the dye adsorption process (such as RB), MCM-41 may be an effective adsorbent for basic dye removal from aqueous solutions and the adsorption equilibrium data can be well described with the Langmuir model. If basic dyes adsorption introduces a serious disorder in the pore structure of MCM-41 (such as MG and CV), however, the adsorption isotherms will change from type I into type IV and Freundlich model is more appropriate for describing the adsorption equilibrium data than Langmuir model. Thermodynamic calculations indicate that the adsorption of basic dyes on MCM-41 may be an exothermic process. The ΔH^0 for RB, MG, and CV was −32.1, −7.5, and −26.3 kJ/mol, respectively. The adsorption kinetics follows the pseudo-second-order model and the external diffusion is the controlling process.

Acknowledgments

The work was supported by grant NSC 94-2211-E-238-001 of National Science Council (Taiwan, ROC).

References

[1] D. Pokhrel, T. Viraraghavan, Treatment of pulp and paper mill wastewater—a review, Sci. Total Environ. 333 (2004) 37–58.
[2] O. Tünay, I. Kabdasli, G. Eremektar, D. Orhon, Color removal from textile wastewaters, Water Sci. Technol. 34 (1996) 9–16.
[3] A. Cassano, R. Molinari, M. Romano, E. Drioli, Treatment of aqueous effluents of the leather industry by membrane processes: a review, J. Membr. Sci. 181 (2001) 111–126.
[4] H.A. Mekkawy, M.O. Ali, A.M. El-Zawahry, Toxic effect of synthetic and natural food dyes on renal and hepatic functions in rats, Toxicol. Lett. 95 (1998) 155.
[5] K. Srinivasan, M.M. Bhargava, Hepatic binding proteins translocating azo dye carcinogen metabolites from cytoplasm into nucleus in rats, Food Chem. Toxicol. 42 (2004) 503–508.
[6] Z. Sun, Y. Chen, Q. Ke, Y. Yang, J. Yuan, Photocatalytic degradation of a cationic azo dye by TiO_2/bentonite nanocomposite, J. Photochem. Photobiol. A: Chem. 149 (2002) 169–174.
[7] C.C. Wang, L.C. Juang, C.K. Lee, T.C. Hsu, J.F. Lee, H.P. Chao, Effects of exchanged surfactant cations on the pore structure and adsorption characteristics of montmorillonite, J. Colloid Interface Sci. 280 (2004) 27–35.
[8] N.D. Lourenco, J.M. Novais, H.M. Pinheiro, Effect of some operational parameters on textile dye biodegradation in a sequential batch reactor, J. Biotechnol. 89 (2001) 163–174.
[9] G. Crini, Non-conventional low-cost adsorbents for dye removal: a review, Bioresour. Technol. 97 (2006) 1061–1085.
[10] E. Forgacs, T. Cserháti, G. Oros, Removal of synthetic dyes from wastewaters: a review, Environ. Int. 30 (2004) 953–971.
[11] O.G. Rhys, Adsorption on activated carbon-solution to dye waste problems, J. Soc. Dyers Colourists 94 (1978) 293–297.
[12] K.R. Ramakrishna, T. Viraraghavan, Dye removal using low cost adsorbents, Water Sci. Technol. 36 (1997) 189–196.
[13] M. Doğan, M. Alkan, Adsorption kinetics of methyl violet onto perlite, Chemosphere 50 (2003) 517–528.
[14] C.C. Wang, L.C. Juang, T.C. Hsu, C.K. Lee, J.F. Lee, F.C. Huang, Adsorption of basic dyes onto montmorillonite, J. Colloid Interface Sci. 273 (2004) 80–86.
[15] C. Namasivayam, R.T. Yamuna, Adsorption of direct red 12B by biogas residual slurry: equilibrium and rate processes, Environ. Pollut. 89 (1995) 1–7.
[16] S. Netpradit, P. Thiravetyan, S. Towprayoon, Application of 'waste' metal hydroxide sludge for adsorption of azo reactive dyes, Water Res. 37 (2003) 763–772.
[17] T. Robinson, B. Chandran, P. Nigam, Removal of dyes from an artificial textile dye effluent by two agricultural waste residues, corncob and barley husk, Environ. Int. 28 (2002) 29–33.
[18] G. Annadurai, R.-S. Juang, D.-J. Lee, Use of cellulose-based wastes for adsorption of dyes from aqueous solutions, J. Hazard. Mater. B92 (2002) 263–274.
[19] M.M. Mohamed, Acid dye removal: comparison of surfactant-modified mesoporous FSM-16 with activated carbon derived from rice husk, J. Colloid Interface Sci. 272 (2004) 28–34.
[20] S. Wang, H. Li, L. Xu, Application of zeolite MCM-22 for basic dye removal from wastewater, J. Colloid Interface Sci. 295 (2006) 71–78.
[21] K.Y. Ho, G. McKay, K.L. Yeung, Selective adsorbents from ordered mesoporous silica, Langmuir 19 (2003) 3019–3024.
[22] J.S. Beck, C. Vartuli, W.J. Roth, M.E. Leonowicz, C.T. Kresge, K.D. Scmmitt, C.T-W. Chu, D.H. Olson, E.W. Sheppard, S.B. McCullen, J.B. Higgins, J.L. Schlenker, A new family of mesoporous molecular sieves prepared with liquid crystal templates, J. Am. Chem. Soc. 114 (1992) 10834–10843.
[23] J. Wloch, M. Rozwadowski, M. Lezanska, K. Erdmann, Analysis of the pore structure of the MCM-41 materials, Appl. Surf. Sci. 191 (2002) 368–374.
[24] S. Muto, H. Imai, Relationship between mesostructures and pH conditions for the formation of silica–cationic surfactant complexes, Micropor. Mesopor. Mater. 95 (2006) 200–205.
[25] C. Kaewprasit, E. Hequet, N. Abidi, J.P. Gourlot, Application of methylene blue adsorption to cotton fiber specific surface area measurement: part I. Methodology, J. Cotton Sci. 2 (1998) 164–173.
[26] D. Lia, W. Zhaoa, X. Suna, J. Zhanga, M. Anpob, J. Zhao, Photophysical properties of coumarin derivatives incorporated in MCM-41, Dyes Pigments 68 (2006) 33–37.
[27] E. Stefan, S. Markus, Immobilization and catalytic properties of perfluorinated ruthenium phthalocyanine complexes in MCM-41-type molecular sieves, Micropor. Mesopor. Mater. 27 (1999) 355–363.
[28] G. Gu, P.P. Ong, C. Chu, Thermal stability of mesoporous silica molecular sieve, J. Phys. Chem. Solids 60 (1999) 943–947.
[29] M. Kruk, M. Jaroniec, A. Sayari, Structural and surface properties of siliceous and titanium-modified HMS molecular sieves, Mesopor. Mater. 9 (1997) 173–182.
[30] I. Langmuir, The adsorption of gases on plane surface of glass, mica and platinum, J. Am. Chem. Soc. 40 (1918) 1361–1368.
[31] H.M.F. Freundlich, Over the adsorption in solution, Z. Phys. Chem. 57 (1906) 385–470.
[32] D.M. Ruthven, Principles of Adsorption and Adsorption Processes, Wiley, New York, 1984, p. 44.
[33] S. Azizian, Kinetic models of sorption: a theoretical analysis, J. Colloid Interface Sci. 276 (2004) 47–52.
[34] G.E. Boyd, A.W. Adamson, L.S. Myers Jr., The exchange adsorption of ions from aqueous solutions by organic zeolites. II. Kinetics, J. Am. Chem. Soc. 69 (1947) 2836–2848.
[35] V. Vadivelan, K.V. Kumar, Equilibrium, kinetics, mechanism, and process design for the sorption of methylene blue onto rice husk, J. Colloid Interface Sci. 286 (2005) 90–100.
[36] K.P. Sing, D. Mohan, S. Sinha, G.S. Tondon, D. Gosh, Color removal from wastewater using low-cost activated carbon derived from agricultural waste material, Ind. Eng. Chem. Res. 42 (2003) 1965–1976.
[37] K.V. Kumar, V. Ramamurthi, S. Sivanesan, Modeling the mechanism involved during the sorption of methylene blue onto fly ash, J. Colloid Interface Sci. 284 (2005) 14–21.